ELSEVIER

International Journal of Mass Spectrometry and Ion Processes 174 (1998) 81–94

International Journal of Mass Spectrometry and Ion Processes

Surface-induced dissociation of diphenyl ether

Janine de Maaijer-Gielbert[a,*], Árpád Somogyi[b], Vicki H. Wysocki[b], Piet G. Kistemaker[a], Tina L. Weeding[a]

[a]*FOM-Institute for Atomic and Molecular Physics, Kruislaan 407, 1098 SJ Amsterdam, The Netherlands*
[b]*Department of Chemistry, University of Arizona, Tucson, AZ 85721-0041, USA*

Abstract

The primary fragmentation of diphenyl ether and further secondary dissociation of its fragments have been studied by surface-induced dissociation (SID). In a tandem linear time-of-flight mass spectrometer, the dissociation of ions is studied as a function of the collision energy with a liquid perfluorinated polyether (PFPE) surface. In a tandem quadrupole instrument, an alkyl terminated (C_{18}) and a perfluoroalkyl terminated (FC_{10}) self-assembled monolayer surface have been used. The differences in the spectra obtained with the TOF and quadrupole instruments are attributed to the different time frames available for observation of the fragments. Deconvolution of the collision energy resolved SID spectra of diphenyl ether shows that above 50 eV collision energy, the energy deposition efficiency is similar in the two experimental set-ups, in spite of the different geometries. Ion/surface reactions are observed upon collisions of the diphenyl ether radical cation with the C_{18} surface but not with the FC_{10} surface The rearrangement fragments, obtained from perdeuterated diphenyl ether, $C_{11}D_{10}^+$ and $C_{11}D_9^+$, react with both the C_{18} and FC_{10} surface. Hydrogen exchange with the surface combined with hydrocarbon loss from $C_{12}D_{10}O^+$, $C_{11}D_{10}^+$, and $C_{11}D_9^+$ is observed. © 1998 Elsevier Science B.V.

Keywords: Surface-induced dissociation; Diphenyl ether; Ion/surface reactions; Self-assembled monolayer; Energy conversion efficiency

1. Introduction

During the last 10–15 years, surface-induced dissociation (SID) has been employed as a tool in analytical mass spectrometry to deposit a well-defined amount of energy into many different types of ions [1–5]. For recent reviews, see Refs. [4,6–8]. For SID, low-energy (0–200 eV, but usually below 100 eV) collisions are sufficient to overcome the activation energies for fragmentation of most types of ions. Different types of mass spectrometers have been used in which SID is implemented, in varying geometries. Examples are sector [9,10], quadrupole [2,11], time of flight [7,12], ion trap [13] and Fourier-transform mass spectrometers [14–16].

An important characteristic of SID is the defined internal energy deposition in the ion, which can be tuned by varying the laboratory collision energy. Many of the species which have been employed to quantify the energy deposition in ion/surface collisions are small ions such as metal carbonyls ('thermometer molecules') [2,4,17] and benzene radical cations [5,18]. These ions show their most informative fragments between 10 and 80 eV collision energies. Kinetic into internal energy conversion efficiencies of 12–18% for hydrocarbon covered

* Corresponding author.

PII S0168-1176(97)00292-9

surfaces [2,17], and 18–30% for fluorinated surfaces [4,5,17,18] have been reported. Systematically, the lower value corresponds to the 'thermometer molecule' method, the higher value to the benzene deconvolution method. For the fragmentation of large or especially stable species, such as peptides [8] and buckminsterfullerenes [7], the required collision energies may extend to 100 eV or more. In this paper, ion/surface collisions of the diphenyl ether radical cation and two of its fragments are investigated. Diphenyl ether is small enough to show distinct fragments at collision energies lower than 30 eV, but on the other hand is stable enough to show informative changes in fragmentation at collision energies higher than 100 eV. In addition to hydrogen atom loss, the diphenyl ether radical cation ($C_{12}H_{10}O^{+\cdot}$) shows two main fragmentation channels: a rearrangement reaction that involves CO loss, presumably leading to a benzotropylium radical cation ($C_{11}H_{10}^{+\cdot}$), and a direct cleavage, presumably leading to a phenyl cation ($C_6H_5^+$), both of which can in turn fragment further [19,20]. The appearance energies for the $C_{11}H_{10}^{+\cdot}$ and $C_6H_5^+$ fragments have been reported previously to be 12.69 and 14.88 eV, respectively [20]. The secondary fragmentation of $C_6H_5^+$ is expected to show several fragments which also occur in the fragment spectra of benzene. Benzene has been employed to quantify the internal energy deposition by alkyl and fluoroalkyl collision surfaces, for up to 80 eV kinetic energy of the projectile ions [2,5,18]. Since diphenyl ether is larger than benzene and several eV are required to form $C_6H_5^+$, it is expected that relatively high internal energies will be required to show similar fragments as benzene.

In addition to fragmentation, ion/surface reactions have been observed for a wide variety of colliding ions, and on different types of surfaces [17,21–30]. The nature and extent of the ion/surface reactions observed depends strongly on the nature of the colliding ion and the composition of the surface. For example, upon collisions with a hydrocarbon surface, acetone, DMSO and pyridine radical cations give extensive H addition reactions and can be used to probe surface damage and/or surface contamination [25]. It has been shown that benzene radical cations give a higher abundance of methyl adducts than doubly charged benzene ions, while they give about the same abundances of ions corresponding to F additions [26]. For isomeric $C_6H_6^{+\cdot}$ ions, Hayward et al. have shown that the benzene radical cation gives more extensive methyl adducts upon collision with a stainless steel surface covered with pump-oil residues, than 1,5-hexadiyne or 2,4-hexadiyne radical cations [22]. Extensive ion/surface reactions with respect to alkyl addition are obtained from collisions of pyrene radical cations with stainless steel or alkyl self-assembled monolayer surfaces [17,31]. Diphenyl ether as an aromatic radical cation is expected to show some reactivity towards an alkyl collision surface.

In this paper, we show the use of diphenyl ether as a probe to estimate the internal energy deposition efficiency at collision energies of more than 100 eV. Furthermore, we have compared the SID fragment spectra of the diphenyl ether radical cation acquired on two different instruments: a tandem TOF and a tandem quadrupole mass spectrometer. These instruments differ in geometry and in the time frame during which fragmentation can be probed. In addition, we have investigated the ion/surface reactions of the diphenyl ether radical cations and of the CO loss rearrangement fragments with C_{18} and FC_{10} surfaces.

2. Experimental

The tandem linear time-of-flight mass spectrometer has been described in detail earlier [18] The ions are selected in the first time-of-flight section which is approximately normal to the collision surface; the SID-fragments are identified based on their flight times in the second stage between the surface and the detector. The collision energy is defined by

the potential energy difference between the point of ionization and the collision surface, and can be tuned by varying the voltage on the surface. The energy of the ions at the laser focus is approximately 3 keV and depends on the start position in the extraction field (0.3 kV/cm). This position is know within ± 0.5 mm, which leads to an uncertainty of ± 15 eV. The potential energy is verified experimentally by lowering the voltage on the collision surface until the signal of the parent ions starts to decrease, due to the onset of ion/surface collisions. We estimate the uncertainty in the collision energy scale as ± 10 eV. The width of the ionizing laser beam at the focal point of the lens is about 90 μm, which results in a kinetic energy distribution of ± 1.5 eV in the parent ion beam.

The gas-phase diphenyl ether molecules are introduced into the ionization chamber through a skimmer, after cooling in a supersonic expansion from a pulsed nozzle which is heated to about 40°C. Ionization is performed in a 1 + 1 resonance enhanced multiphoton process with 4.46 eV photons. The total energy available in this two-photon process leaves a maximum of 0.89 eV for the internal energy of the radical cations if the energy in excess of the ionization threshold, determined from the photoelectron spectrum as 8.03 ± 0.15 eV [32] were to remain in the ion. The laser light of about 2 mJ per pulse is focused into the ion source by a cylindrical lens (focal length 15 cm). For the SID experiments, formation of the $C_6H_5^+$ fragment ions is accomplished upon absorption of two additional photons by the diphenyl ether radical cation. This leaves the fragment with a maximum of 1.5 eV internal energy, if upon ionization of diphenyl ether all the excess energy were to remain in the diphenyl ether radical cation, and if upon photodissociation the excess energy were equally distributed among the degrees of freedom (DOF) of the fragment ion and the neutral. Interference of other ions than the intended parent ion created in the ion source, with fragments obtained by surface-induced dissociation, is avoided by pulsing the voltage on the collision surface [18]. The collision surface consists of a stainless steel plate covered by a thin film of high molecular weight liquid perfluorinated polyether (PFPE), as described earlier [18]. The geometrical angle defined by the ion source, collision surface and detector is about 6°, resulting in a geometrical angle of incidence of the ions with respect to the surface normal of 3°. Yeretzian et al. have discussed how the angle of incidence of the ions changes because the ratio of the parallel and perpendicular velocity of the ions is changed by the deceleration at the surface, but they have observed little change in fragmentation patterns by varying this angle [7].

The tandem quadrupole instrument used has been described earlier [2]. Briefly, it consists of two 4000 u quadrupoles (Extrel, Pittsburgh, PA) arranged in a 90° geometry with the surface positioned to intersect the ion optical path of each quadrupole. The angle between the ion beam and the surface normal is kept at 45 ± 5°. The diphenyl ether molecules are brought into the ion source by heating the sample vessel and inlet tube (about 40°C) and ionized by 70 eV electron impact. The collision surfaces utilized are self-assembled monolayers (SAMs) from alkyl thiols grown on clean vapour-deposited gold surfaces. The experiments described below utilize SAM-surfaces consisting either of hydrogen terminated alkyl chains with 18 carbon atoms (C_{18} surface) or of fluorine-terminated alkyl chains, CF_3-$(CF_2)_7$-$(CH_2)_2$-S-Au, (FC_{10} surface). The efficiency of charge retention at these surfaces has been reported previously [27] and is higher for the fluorocarbon surface than for the hydrocarbon surface (65% vs. 12%, respectively, with benzene projectile).

For gas-phase collision activated dissociation (CAD) experiments, a JEOL SX-102 double focusing mass spectrometer is used. A 10 keV parent ion beam formed by 70 eV electron impact enters the collision cell filled with helium. This collision cell is positioned between the magnetic sector, which is used for selection of the parent ions, and the

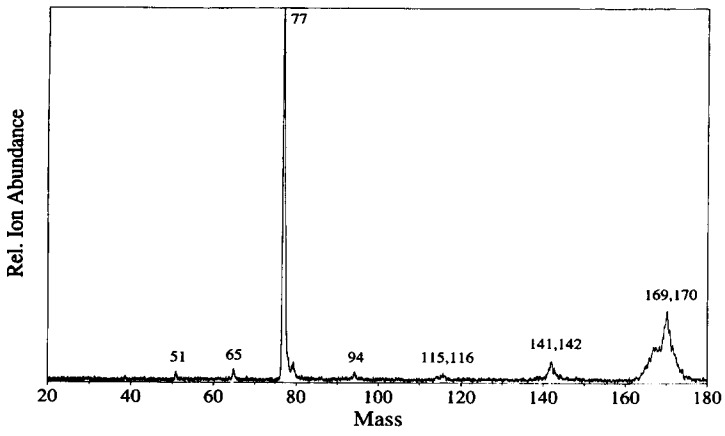

Fig. 1. 20 eV SID spectrum of the radical cation of diphenyl ether on a PFPE surface in the tandem TOF instrument. This spectrum is acquired from 1250 laser shots.

electrostatic analyzer, which is scanned to obtain the fragment spectrum (CAD-MIKE experiments).

3. Results and discussion

3.1. Spectra and ER-SID diagrams

Fig. 1 shows the SID spectrum that results from 20 eV collisions of diphenyl ether radical cation (*m/z* 170) with a PFPE surface in the tandem TOF mass spectrometer, an instrument in which the resolution is limited to about 100 at *m/z* 100 [18]. Fig. 2 shows a plot of the relative fragment ion intensities of diphenyl ether as a function of the collision energy in the tandem TOF mass spectrometer. Energy-resolved SID diagrams (ER-SID) of this type are useful to

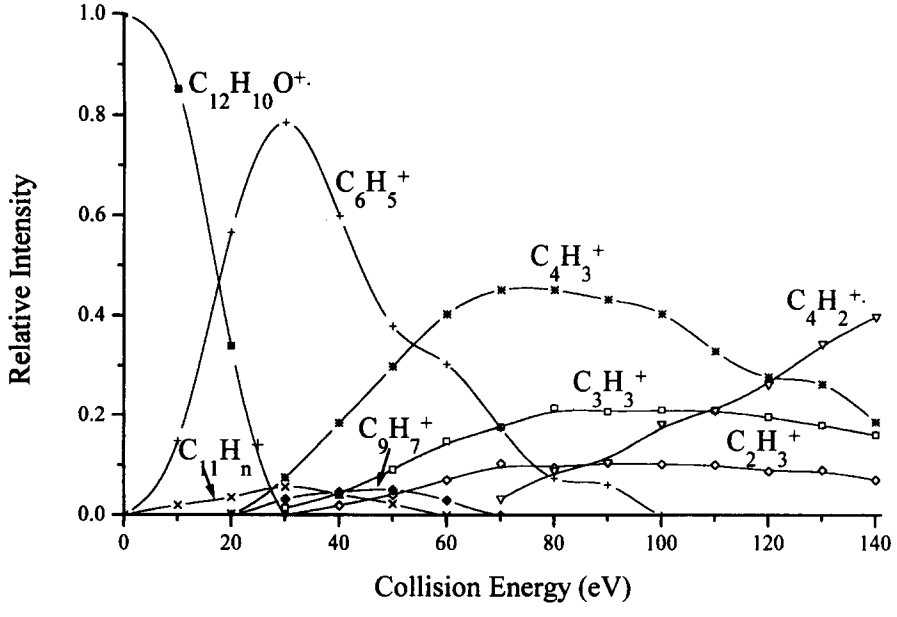

Fig. 2. ER-SID diagram of the radical cation of diphenyl ether on the PFPE collision surface. Only the fragments with an abundance of more than 10% at any collision energy are indicated. The spectra on which this diagram is based are acquired from 1250 laser shots.

monitor dissociation pathways as a function of collision energy. Note that ER-SID diagrams should be distinguished from breakdown diagrams which show relative fragment ion intensity as a function of the (univalue) internal energy. As indicated by the spectrum (Fig. 1) and the ER-SID diagram (Fig. 2), at collision energies lower than 50 eV the dominant fragment ion is the direct cleavage product $C_6H_5^+$ at *m/z* 77. Further fragmentation of $C_6H_5^+$ (see discussion below) accounts for the dominant ions in the low *m/z* range (lower than *m/z* 77) at higher collision energies. In contrast to the high intensity of the direct cleavage product, the expected CO loss rearrangement product, $C_{11}H_{10}^+$ (*m/z* 142), is of low intensity even at low collision energies. Also notable in Fig. 1 is the signal of fragments from metastable decay in the first field free region. These fragments appear around *m/z* 165 in the SID spectrum and inhibit the accurate determination of the intensity of the SID fragment ions in this mass range.

Fig. 3 shows the 20 eV SID spectrum of diphenyl ether colliding with a FC_{10} surface in the tandem quadrupole instrument [33]. The acquisition time of this spectrum is comparable to the time required to obtain the TOF SID spectrum in Fig. 1, which is about 10 min. From a comparison of the spectra in Fig. 1 and Fig. 3 it is clear that the tandem quadrupole instrument yields a much better signal-to-noise ratio than the tandem TOF. This is expected based on the difference in parent ion current, estimated as 10^4 ions/s for the tandem TOF, and 10^9 for the tandem quadrupole. Furthermore, the tandem quadrupole yields a better resolution above *m/z* 100. Fig. 4 shows the ER-SID diagrams recorded with the tandem quadrupole instrument. Some ER-SID curves look similar obtained with the tandem TOF and the tandem quadrupole instruments (using fluorinated surfaces), e.g. compare the curves of $C_6H_5^+$ and $C_4H_3^+$ in Fig. 2 with those in Fig. 4(a). Other curves are clearly different, especially those related to the CO loss rearrangement products. Due to the limited resolution we use the summed signal of the rearrangement fragments $C_{11}H_n^+$ ($n = 7–10$, *m/z* 139–142) for the ER-SID diagram in Fig. 2. The rearrangement fragment $C_{11}H_{10}^+$ should have its maximum intensity at SID collision energies between 15 and 25 eV when one assumes that the time frame for dissociation is of the same order of magnitude as that used to measure the appearance energy for this fragment. This is based on estimates of the efficiency of conversion of collision energy into internal energy (about 30% for the PFPE surface [18]), and the 4.66 eV difference between the known ionization energy (8.03 eV [32]) for the

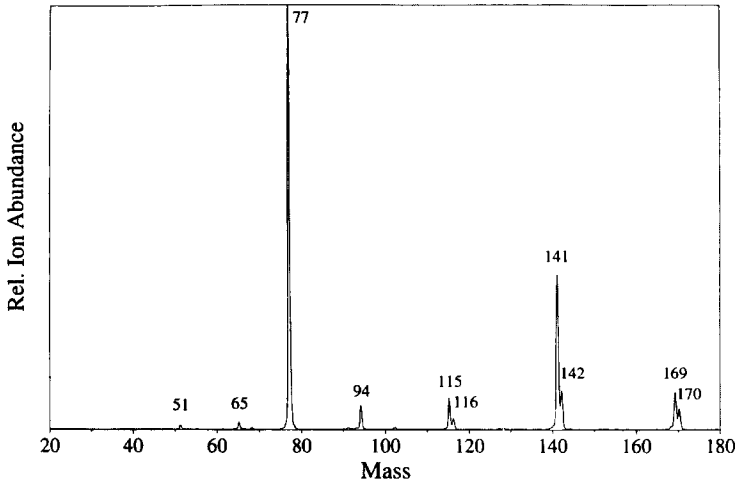

Fig. 3. 20 eV SID spectrum of the radical cation of diphenyl ether on a FC_{10} surface in the tandem quadrupole instrument.

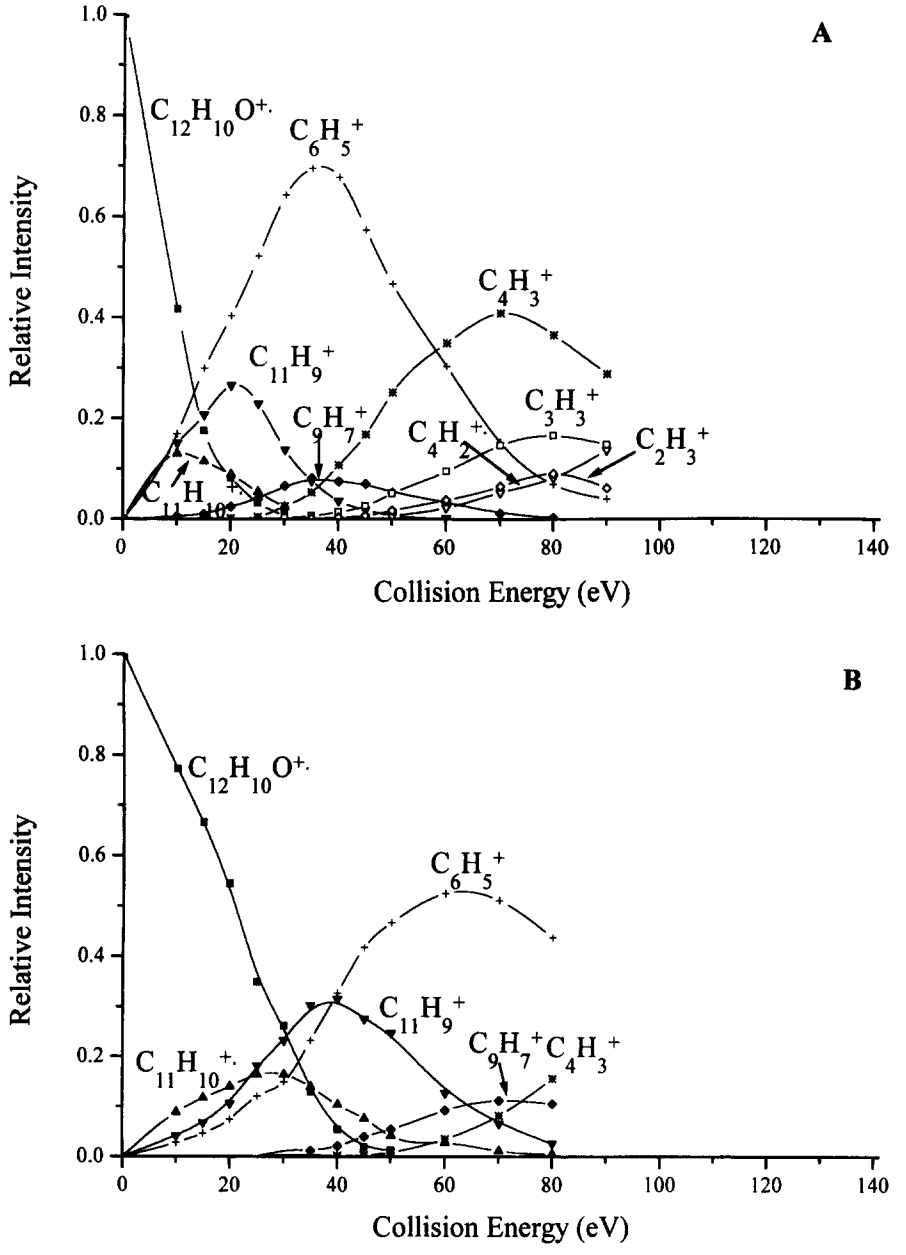

Fig. 4. (a) ER-SID diagram of the radical cation of diphenyl ether on the FC_{10} surface showing only fragments with an abundance > 10%. (b) ER-SID diagram of the radical cation of diphenyl ether on C_{18} surface. Only with low energy deposition and at low collision energies, the fragment $C_{11}H^{+}_{10}$ (*m/z* 142) is the most abundant fragment.

parent ion and appearance energy (12.69 eV [19]) for the fragment ion. For the direct cleavage product $C_6H_5^+$, the appearance energy has been established as 14.88 eV [19] leading to a AE-IE value of 6.85 eV. Although the rearrangement fragments are present at collision energies between 15 and 25 eV, in the TOF-SID spectra their abundance is never higher than the abundance of the fragment formed by direct cleavage, $C_6H_5^+$, even at 10 eV collision energy.

We attribute this to a combination of the width of the distribution of internal energy deposition, and the short time frame for observation of the rearrangement reaction in the TOF-SID instrument. The length of the acceleration region after the collision surface is 10 mm in the TOF-SID instrument. Combined with an acceleration voltage of 3 kV, this results in a time spent in the acceleration section of only 0.2 μs for an ion of *m/z* 100. In the tandem quadrupole instrument this time frame is about 2 μs and therefore the relative intensity of the fragments connected with CO loss is higher. It is difficult to tune the tandem quadrupole instrument at a collision energy lower than 10 eV, so that $C_{11}H_{10}^{+\cdot}$ ions are never the most abundant fragments in the experiments performed with the FC_{10} surface. When the C_{18} surface is used, the $C_{11}H_{10}^{+\cdot}$ ions are the most abundant fragments between 10 and 20 eV collision energy (Fig. 4(b)), which is consistent with the smaller kinetic into internal energy conversion efficiency for the C_{18} surface [5,17]. These results show that the differences in the ER-SID curves are related to the differences in the observation time for the two instruments. In its current configuration, the tandem TOF instrument cannot be used to study fragmentation processes which occur on a microsecond time scale. This could be advantageous for systems in which rearrangements complicate interpretation of the mass spectrum. A possible improvement to allow investigation of slower dissociations would involve delayed extraction of the fragments after the collision surface. Since the ER-SID curves of the fragments from the direct cleavage reaction are very similar, we conclude that for the higher-energy collisions ($\geq$50 eV), the difference in geometry between the instruments (6° vs. 90°, collisions at 90° vs. 45°; see Section 2) does not greatly influence the internal energy deposition by the fluorinated alkyl surface. This has already been indicated by experiments with benzene [18] and scattering experiments of CF_3^+ [34].

SID experiments with the $C_{11}H_{10}^{+\cdot}$ and $C_{11}H_9^+$ ions are performed in the tandem quadrupole instrument. To improve the mass selection of the parent ion, and to investigate possible ion/surface reactions, perdeuterated diphenyl ether is used for these experiments. These experiments were compared with keV CAD experiments of selected $C_{11}H_{10}^{+\cdot}$ formed from $C_{12}H_{10}O^{+\cdot}$, as summarized below:

$$C_{12}H_{10}O^{+\cdot} \xrightarrow[\text{EI}]{-CO} C_{11}H_{10}^{+\cdot} \xrightarrow[\text{SID or CAD}]{-H}$$

$$\rightarrow C_{11}H_9^+ \xrightarrow{-C_2H_2} C_9H_7^+ \rightarrow m/z\ 89,\ 65\ \text{etc.}$$

$C_{11}D_9^+$ ($C_{11}H_9^+$) is a dominant product of $C_{11}D_{10}^{+\cdot}$ ($C_{11}H_{10}^{+\cdot}$). This is in contrast to the CAD results reported by Stiller and Johnston [20] who found that $C_{11}H_9^+$ was not formed from $C_{11}H_{10}^{+\cdot}$. Acetylene loss from $C_{11}D_{10}^{+\cdot}$ ($C_{11}H_{10}^{+\cdot}$) resulting in $C_9D_8^{+\cdot}$ ($C_9H_8^{+\cdot}$) (*m/z* 124 (116)) is observed only in small (< 2%) amounts from SID on FC_{10} or the CAD experiments.

Table 1 contains a list of all fragments of the diphenyl ether radical cation which appear with a peak height of at least 0.1% in any of the tandem quadrupole and 1% in the tandem TOF SID spectra, along with a proposal for their formation. SID experiments with the (perdeuterated) rearrangement fragments have been used to confirm the composition of some of the fragments. The relative peak height of a fragment at the collision energy (below 140 eV) corresponding to its maximal abundance, is qualified with S (strong) when between 5 and 100%, M (medium) when between 1 and 5% and W (weak) when between 0.1 and 1%. Table 1 shows, for example, that if sufficient energy is imparted in the rearrangement fragments $C_{11}D_{10}^{+\cdot}$ and $C_{11}D_9^+$, a small amount of $C_6D_5^+$ is formed. This reaction however is not expected to contribute to the amount of $C_6H_5^+$ formed from the diphenyl ether radical cation, due to the competitive shift.

3.2. Estimate of internal energy deposition

Vékey et al. have determined the internal

energy deposition for benzene radical cations upon SID in the collision energy range of 10–70 eV [5]. The ER-SID diagram was deconvoluted with the use of a breakdown diagram for benzene, as obtained by photodissociation experiments. However, to our knowledge, no breakdown diagrams have been published for diphenyl ether which extend to the high internal energies as deposited by the ion/surface collisions. Brown has obtained ratios of the rearrangement and cleavage reactions of diphenyl ether as a function of the EI energy [19]. At SID collision energies higher than 50 eV, the fragment ion spectrum of diphenyl ether is dominated by the primary fragment $C_6H_5^+$ (*m/z* 77) and the secondary products of this fragment $C_4H_3^+$ (*m/z* 51) and $C_4H_2^{+\cdot}$ (*m/z* 50). This opens the possibility to use these secondary fragment ions to estimate the energy deposition into the diphenyl ether radical cation. The other fragments on which the deconvolution of the ER-SID diagram of benzene is based, C_3H^+ (*m/z* 37) and $C_2H_2^{+\cdot}$ (*m/z* 26), appear with such low abundances in the TOF-SID spectra of diphenyl ether, that they are not included. Furthermore it can be argued that other fragmentation pathways give only minor contributions to the formation of $C_4H_3^+$ and $C_4H_2^{+\cdot}$ ions from diphenyl ether. It is assumed that after the primary fragmentation the residual internal energy is distributed over the secondary fragments in proportion to their degrees of freedom (DOF). On the basis of this assumption, the energy deposited into the parent diphenyl ether ion can be calculated from the internal energy of the primary fragment ion $C_6H_5^+$, as calculated from the relative intensities of the secondary fragments

Table 1
Summary of fragments observed upon SID of the diphenyl ether radical cation. The second column (*I*) indicates the maximum intensity at any collision energy between 10 and 140 eV: S (strong) when between 5 and 100%, M (medium) when between 1 and 5% and W (weak) when between 0.1 and 1%. The third and fourth columns show the atomic composition and a proposal for the origin of the fragment. The fifth column shows the mass-to-charge ratio at which the equivalent fragment from perdeuterated diphenyl ether is observed upon collisions with a fluorinated alkyl surface. The last column shows which fragment of diphenyl ether was used to confirm the composition of the fragment in the second column

m/z	*I*	Formula	Process	H → D (*m/z*)	Confirmed by SID of
170[t,q]	S	$C_{12}H_{10}O$	M	180	$C_{12}D_{10}O$
169[t,q]	M	$C_{12}H_9O$	M–H	178	$C_{12}D_{10}O$
168[q]	M	$C_{12}H_8O$	M–H_2	176	$C_{12}D_{10}O$
155[q]	M	$C_{11}H_7O$	M–CH_3	162	$C_{12}D_{10}O$
153[q]	W	$C_{11}H_5O$	155–H_2	158	$C_{12}D_{10}O$
152[q]	W				
151[q]	W				
144[q]	W				
142[t,q]	S	$C_{11}H_{10}$	M-CO	152	$C_{11}D_{10}$
141[t,q]	S	$C_{11}H_9$	142–H, 169–CO	150	$C_{11}D_{10}$, $C_{11}D_9$
140[q]	W	$C_{11}H_8$			
139[q]	M	$C_{11}H_7$	141–H_2	146	$C_{11}D_{10}$, $C_{11}D_9$
131[q]	W	C_9H_7O	M–C_3H_3	138	$C_{12}D_{10}O$
129[q]	W	C_9H_5O	155–C_2H_2	134	$C_{12}D_{10}O$
129[q]	W	$C_{10}H_7$	142–CH_3	136	$C_{11}D_{10}$, ($C_{11}D_9$)[a]
128[q]	W	$C_{10}H_6$	141–CH_3	134	$C_{11}D_{10}$, $C_{11}D_9$
127[q]	W				
126[q]	W				
116[q]	M	C_9H_8	142–C_2H_2	124	$C_{11}D_{10}$
115[t,q]	M	C_9H_7	141–C_2H_2	122	$C_{11}D_9$ (S), $C_{11}D_{10}$ (S)
103[q]	W	C_8H_7	142–C_3H_3	110	$C_{11}D_{10}$
102[q]	M	C_8H_6	141–C_3H_3	108	$C_{11}D_{10}$, $C_{11}D_9$
94[t,q]	M	C_6H_6O	M–C_6H_4		
93[q]	W	C_6H_5O	M–C_6H_5, 94–H		

Table 1
Continued

m/z	I	Formula	Process	H → D (m/z)	Confirmed by SID of
92[q]	W	C_6H_4O	94–H_2		
92[q]	W	C_7H_8	142–C_4H_2	100	$C_{11}D_{10}$ (W), $C_{11}D_9$ (W)[b]
91[q]	M	C_7H_7	141–C_4H_2	98	$C_{11}D_{10}$, $C_{11}D_9$
90[q]	W	C_7H_6	116–C_2H_2	96	$C_{11}D_{10}$ (M), $C_{11}D_9$ (W)[b]
89[q]	M	C_7H_5	115–C_2H_2	94	$C_{11}D_{10}$, $C_{11}D_9$
78[q]	W	C_6H_6	116–C_3H_2	84	$C_{11}D_{10}$ (M), $C_{11}D_9$ (W)[b]
77[t,q]	S	C_6H_5	M–C_6H_5O	84	$C_{12}D_{10}O$
77[t,q]		C_6H_5	116–C_3H_3, 115–C_3H_2	82	$C_{11}D_{10}$ (S), $C_{11}D_9$ (M)
76[q]	W	C_6H_4	77–H		C_6H_5
76[q]	M	C_6H_4	115–C_3H_3	80	$C_{11}D_{10}$ (M), $C_{11}D_9$ (M)
75[q]	M	C_6H_3	77–H_2	78	$C_{11}D_{10}$, $C_{11}D_9$
74[q]	W	C_6H_2	126–C_4H_2	76	$C_{11}D_{10}$, $C_{11}D_9$
70[q]	W				
66[q]	M	C_5H_6	116–C_4H_2	72	$C_{11}D_{10}$
65[t,q]	S	C_5H_5	115–C_4H_2, 91–C_2H_2	70	$C_{11}D_{10}$, $C_{11}D_9$
64[q]	W	C_5H_4	90–C_2H_2	68	$C_{11}D_{10}$
63[t,q]	M	C_5H_3	89–C_2H_2	66	$C_{11}D_{10}$, $C_{11}D_9$
62[q]	W				
55[q]	W				
53[q]	W				
52[q]	W				
51[t,q]	S	C_4H_3	77–C_2H_2		
50[t,q]	S	C_4H_2	77–C_2H_3		
41[q]	W				
40[q]	W				
39[t,q]	S	C_3H_3	94–C_3H_3O	42	$C_{11}D_{10}$, $C_{11}D_9$, C_6H_5 (W)
38[t,q]	M				
37[t,q]	W				
27[t,q]	S	C_2H_3	77–C_4H_2		C_6H_5
26[t,q]	M	C_2H_2	77–C_4H_3		C_6H_5

[t] Tandem TOF SID spectra.
[q] Tandem quadrupole SID spectra.
[a] Only observed with C_{18} surface.
[b] Not expected.

$C_4H_3^+$, $C_4H_2^+$, C_3H^+ and $C_2H_2^+$. To do so, the activation energy for the primary fragmentation of $C_{12}H_{10}O^{+\cdot}$ to $C_6H_5^+$ has to be used. This value is taken to be 6.85 eV, the difference of the appearance energy of $C_6H_5^+$ (14.88 eV) and the ionization energy of $C_{12}H_6O^{+\cdot}$ (8.03 eV) [19]. No correction is made for the kinetic shift.

$$E_{int}(C_{12}H_{10}O^{+\cdot}) = 6.85 + 7/3 \times E_{int}(C_6H_5^+)$$

Note that our present approach is similar to that of Meot-Ner (Mautner) et al. who have compared the SID fragmentation of protonated leucine-enkephalin (YGGFL) and its proton-bound dimer by correcting for the DOF ratio and hydrogen bond energy [35].

We have applied this adapted deconvolution both to the SID spectra of the diphenyl ether radical cation obtained with the tandem TOF and to those obtained with the tandem quadrupole SID instruments. Furthermore, to verify whether the deconvolution of fragment spectra of $C_6H_6^+$ can be applied to $C_6H_5^+$, we have obtained and deconvoluted SID spectra of $C_6H_5^+$. The results are shown in Fig. 5 in which the mean internal energy is plotted versus the collision energy. The uncertainty in the data

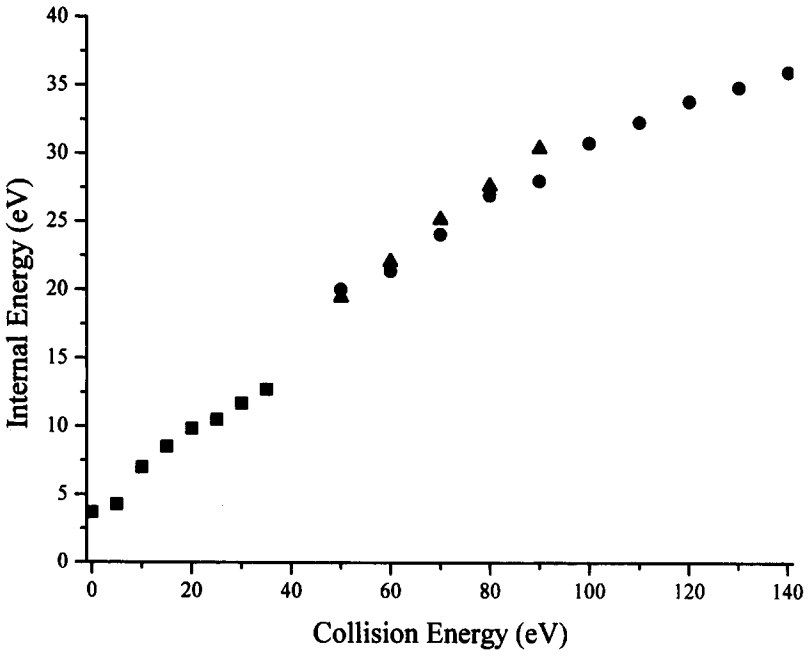

Fig. 5. Plot of the average energy deposited into the parent ions on fluorinated surfaces, calculated by deconvolution of the (further) fragments of $C_6H_5^+$ versus collision energy. ■, $C_6H_5^+$; ▲, $C_{12}H_{10}O^{+\cdot}$ in tandem TOF; ●, $C_{12}H_{10}O^{+\cdot}$ in tandem quadrupole.

points obtained for the tandem TOF is somewhat larger than for the tandem quadrupole: due to signal/noise limitations we estimate an uncertainty of about 10% in the determination of the peak area in the TOF spectra, leading to an uncertainty in the calculated average energy deposited of ± 0.3 eV.

From Fig. 5 it appears that the data points from $C_6H_5^+$ and those from the diphenyl ether fragmentation observed with the quadrupole, are on one line. The TOF data appear to level off at collision energies higher than 80 eV. For the collision energies of 80 eV and lower, the estimated deposited energies are similar to those obtained from the tandem quadrupole spectra. The leveling off may be a consequence of the omission of the high energy fragments C_3H^+ and $C_2H_2^{+\cdot}$ for the deconvolution, which is also shown to occur for benzene by Vékey et al. [5]. A linear fit through the data points for $C_{12}H_{10}O^{+\cdot}$ has a slope of 0.27 for the tandem quadrupole and 0.24 for the linear part of the tandem TOF data, implying internal energy conversion efficiencies of 27% and 24% for fluorinated surfaces, respectively. For SID spectra obtained for $C_6H_5^+$ on the TOF instrument a conversion efficiency of 27% is obtained. This value is comparable to the 28% obtained by deconvolution of the SID spectra of the benzene radical cation for the tandem quadrupole by Vékey et al. [5] and the (30 ± 7)% for the tandem TOF [18]. The result for $C_6H_5^+$ gives us confidence that, within the assumptions made, the derived energy deposition for diphenyl ether shows the expected tendency. Further work is required to understand the value of the *y*-intercept in Fig. 5.

Note that the results of this adapted deconvolution are not reliable when a large part of the distribution of internal energies deposited is lower than the formation energy of $C_6H_5^+$ from $C_{12}H_6O^{+\cdot}$. The internal energy distribution curves obtained by Vékey et al. for benzene show that at 50 eV collision energy, only a few percent of the ions obtain an internal energy lower than about 7 eV [5]. For 30 eV collisions the amount is significantly higher. Therefore we have restricted ourselves to SID spectra acquired at collision

energies of 50 eV and higher for our estimate of the average energies deposited. To accurately calculate the internal energy distribution deposited into the diphenyl ether radical cations and hence the conversion efficiency of kinetic into internal energy, comparison with a breakdown diagram of diphenyl ether radical cations would be required, or another method or molecule could be used to compare the average energy deposition for the two instruments.

3.3. Ion/surface reactions

Collision of the diphenyl ether radical cation with the C_{18} surface results in peaks at *m/z* 183 ($C_{12}H_{10}O^{+\cdot} + CH_3 - H_2$) and at *m/z* 197 ($+CH_2CH_3 - H_2$), reactions which have also been observed for benzene [27]. However, for the FC_{10} surface, no reaction products have been observed at *m/z* 187 (+ F $-H_2$), where they are expected in analogy with the behaviour of benzene radical cations [27]. The reaction products formed upon collision with the C_{18} surface are confirmed by experiments with the perdeuterated compound. The ion/surface reactions observed are shown in Scheme 1. In addition, ion/surface collisions of the perdeuterated radical cation with the C_{18} surface leads to odd-mass peaks at *m/z* 161, 159, 135, 97 and 69 (Fig. 6(a)), while in the SID spectra on the FC_{10} surface only the even mass fragment peaks around these *m/z* values are present (Fig. 6(b)). For formation of the odd-mass products we propose a mechanism which involves hydrogen addition followed by the loss of a hydrocarbon neutral.

To compare the reactivity of the diphenyl ether radical cation with that of its primary fragments towards these surfaces, we have obtained SID spectra of the perdeuterated rearrangement fragments (Fig. 6(c)–(f)). In the spectra of both $C_{11}D^{\oplus}_{10}$ and $C_{11}D_9^+$, colliding with the C_{18} surface, addition products at *m/z* 165 ($+CH_3 - H_2$), 164, 163 etc., are observed. Methyl loss from $C_{11}D^{\oplus}_{10}$ and $C_{11}D_9^+$ is accompanied by ion/surface reactions with the C_{18}-surface, yielding products at *m/z* 135, 133 and further fragments, depending on the collision energy. The peaks at *m/z* 135, 97 and 69 are also present in the C_{18} SID spectrum of $C_{12}D_{10}O^{+\cdot}$.

The abundance of hydrogen exchange products around *m/z* 135 is lower for $C_{11}D_9^+$ than for $C_{11}D_{10}^+$, while for the SID spectra on the

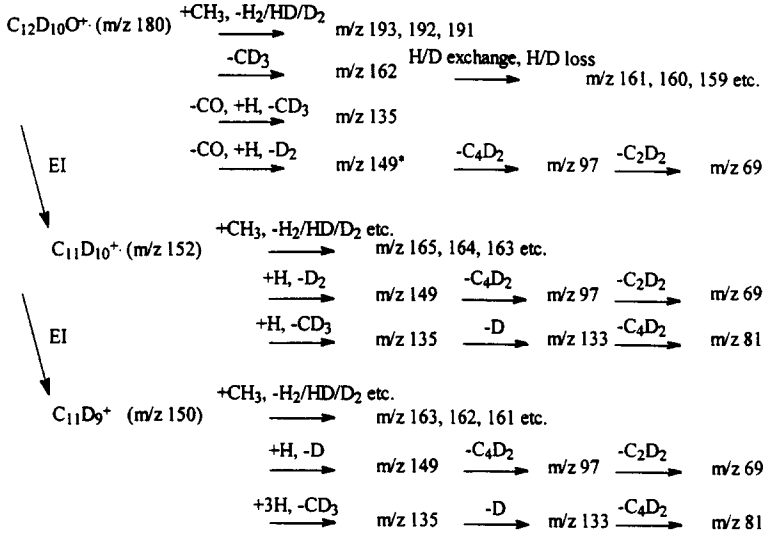

Scheme 1. Ion/surface reactions of perdeuterated diphenyl ether and its CO loss rearrangement fragments with the C_{18} collision surface; * cannot be distinguished in the spectrum.

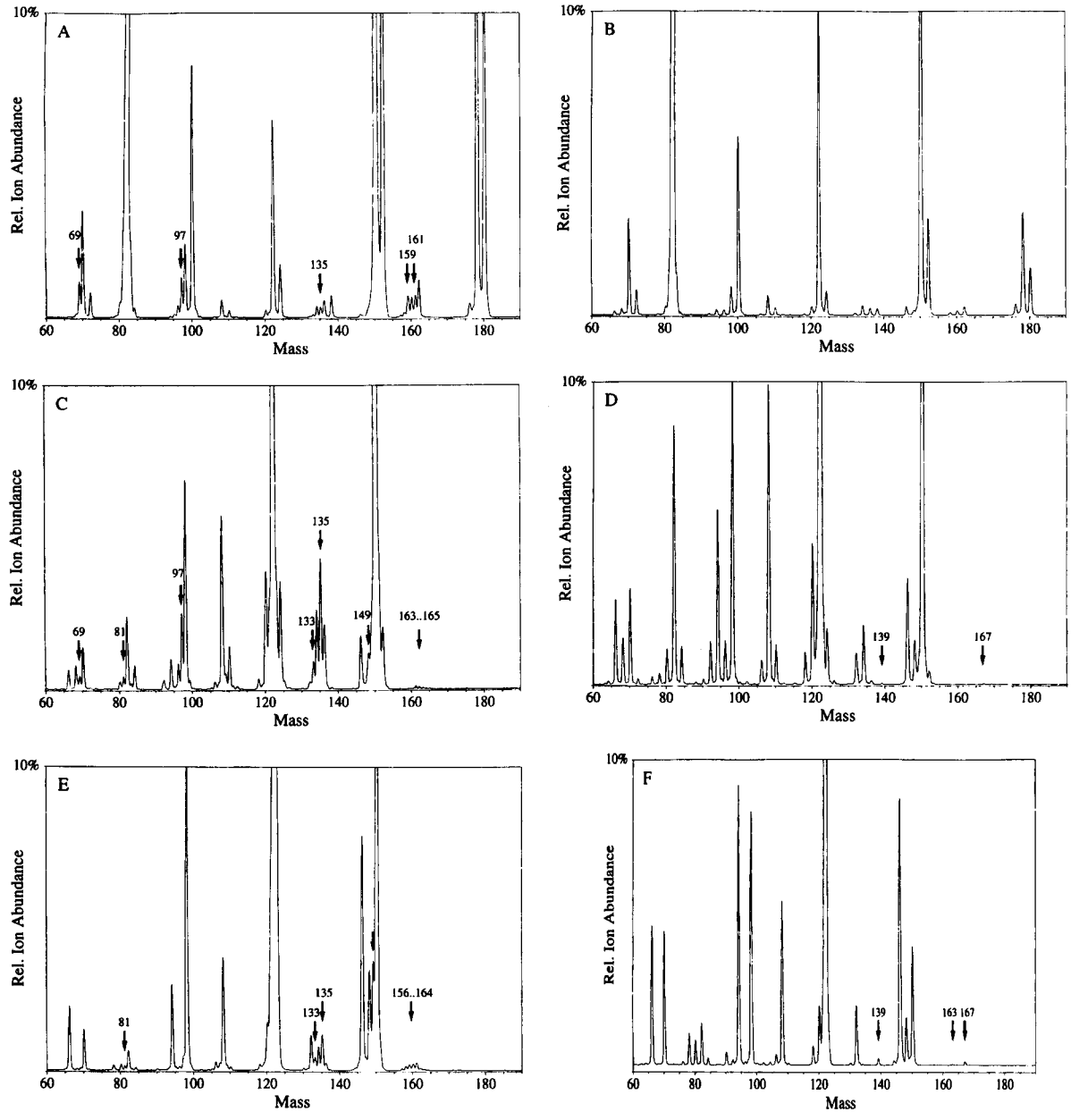

Fig. 6. (a) 40 eV deuterated diphenyl ether on C_{18}; (b) 30 eV deuterated diphenyl ether on FC_{10} surface; (c) 40 eV rearrangement fragment $C_{11}D_{10}^{+}$ on C_{18} surface; (d) 30 eV rearrangement fragment $C_{11}D_{10}^{+}$ on FC_{10}; (e) 40 eV rearrangement fragment $C_{11}D_{9}^{+}$ on C_{18} surface; (f) 30 eV rearrangement fragment $C_{11}D_{9}^{+}$ on FC_{10} surface. The arrows indicate products of ion/surface reactions. Note that the spectra are 10× magnified.

FC_{10} surface, the abundance of the methyl loss fragments (*m/z* 136, 134 and 132) are comparable. This indicates that the reactivity of the odd-electron $C_{11}D_{10}^{+}$ towards direct hydrogen exchange and methyl loss is higher than of the even-electron ion $C_{11}D_{9}^{+}$.

$C_{11}D_{10}^{+}$ and $C_{11}D_{9}^{+}$ show ion/surface reactions with the FC_{10} surface (Fig. 6(d),(f)), while none are observed for diphenyl ether radical cation (Fig. 6(b)). These reactions are summarized in Scheme 2. While the reactivity with the C_{18} surface is different for the odd and even

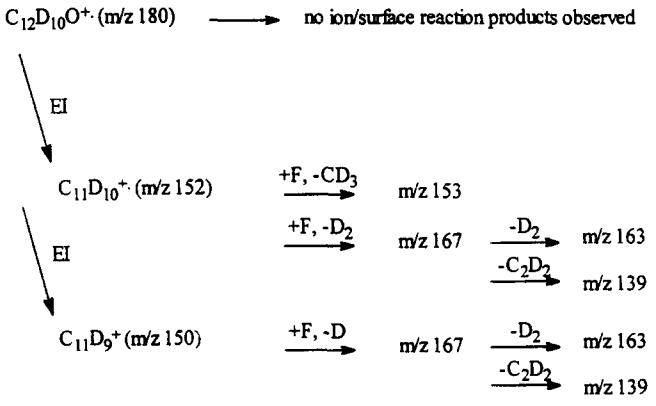

Scheme 2. Ion/surface reactions of perdeuterated diphenyl ether and its CO loss rearrangement fragments with the FC_{10} collision surface.

electron rearrangement fragments, such differences are not so clear for the FC_{10} surface. It must be noted that the overall abundance of ion/surface reaction products is much lower for the FC_{10} surface compared to the C_{18} surface, which makes it more difficult to detect possible differences in reactivity.

4. Conclusions

In spite of the different instrument geometries and collision angles, the tandem linear TOF and the dual quadrupole instruments give similar energy-resolved SID plots for fragmentation of diphenyl ether. The tandem linear TOF has a short time frame (ca. 10^{-7} s) available for observation of fragmentation reactions. This results in general in lower relative intensities of rearrangement fragments than for the tandem quadrupole SID instrument, for which fragments with dissociation times of microseconds can be observed. Deconvolution of energy-resolved SID spectra show that the conversion efficiency of kinetic into internal energy (24–27%) is similar for the two instruments for collisions higher than 50 eV.

Ion/surface reactions of the diphenyl ether radical cation involve hydrocarbon addition combined with hydrogen loss on one hand, and hydrogen addition combined with alkyl loss on the other. The $C_{11}D_{10}^+$ and $C_{11}D_9^+$ fragment ions show more abundant ion/surface reaction products with both the C_{18} and the FC_{10} collision surface, than the perdeuterated diphenyl ether radical cation.

Acknowledgements

The authors would like to thank N.M.M. Nibbering, A.W. Kleyn and W.R. Koppers for helpful discussions, A. Paiva for the photospectroscopic data and J. Pureveen for acquisition of the CAD-MIKE data. This work is performed in collaboration with the Netherlands Foundation for Research on Matter (FOM) with the support (in part) of the Netherlands Technology Foundation (STW). Support of the work at UA by the National Science Foundation, Grant CHE 9224719, is gratefully acknowledged.

References

[1] M.A. Mabud, M.J. DeKrey, R.G. Cooks, Int. J. Mass Spectrom. Ion Proc. 67 (1985) 285.
[2] V.H. Wysocki, J.-M. Ding, J.L. Jones, J.H. Callahan, F.L. King, J. Am. Soc. Mass Spectrom. 3 (1992) 27.
[3] A.L. McCormack, J.L. Jones, V.H. Wysocki, J. Am. Soc. Mass Spectrom. 3 (1992) 859.
[4] T. Pradeep, S.A. Miller, R.G. Cooks, J. Am. Soc. Mass Spectrom. 4 (1993) 769.
[5] K. Vékey, Á. Somogyi., V.H. Wysocki, J. Mass Spectrom. 30 (1995) 212.

[6] R.G. Cooks, T. Ast, M.A. Mabud, Int. J. Mass Spectrom. Ion Proc. 100 (1990) 209.
[7] C. Yeretzian, R.D. Beck, R.L. Whetten, Int. J. Mass Spectrom. Ion Proc. 135 (1994) 79.
[8] A.R. Dongré, Á. Somogyi, V.H. Wysocki, J. Mass Spectrom. 31 (1996) 339.
[9] M.J. DeKrey, M.A. Mabud, R.G. Cooks, Int. J. Mass Spectrom. Ion Proc. 67 (1985) 295.
[10] D. Despeyroux, A.D. Wright, K.R. Jennings, S. Evans, A. Riddoch, Int. J. Mass Spectrom. Ion Proc. 122 (1992) 133.
[11] M.E. Bier, J.W. Amy, R.G. Cooks, J.E.P. Syka, P. Ceja, G. Stafford, Int. J. Mass Spectrom. Ion Proc. 77 (1987) 31.
[12] K. Schey, R.G. Cooks, R. Grix, H. Wöllnik, Int. J. Mass Spectrom. Ion Proc. 77 (1987) 49.
[13] S.A. Lammert, R.G. Cooks, J. Am. Soc. Mass Spectrom. 2 (1991) 487.
[14] E.R. Williams, K.D. Henry, F.W. McLafferty, J. Shabanowitz, D.F. Hunt, J. Am. Soc. Mass Spectrom. 1 (1990) 413.
[15] L.M. Nuwaysir, J.A. Castoro, C.L. Wilkins, Org. Mass Spectrom. 26 (1991) 721.
[16] W. Zhong, E. Nikolaev, J.H. Futrell, V.H. Wysocki, Anal. Chem. 69 (1997) 2496.
[17] M.R. Morris, J.D.E. Riederer, B.E. Winger, R.G. Cooks, T. Ast, C.E.D. Chidsey, Int. J. Mass Spectrom. Ion Proc. 122 (1992) 181.
[18] J. de Maaijer-Gielbert, J.H.M. Beijersbergen, P.G. Kistemaker, T.L. Weeding, Int. J. Mass Spectrom. Ion Proc. 153 (1996) 119.
[19] P. Brown, Org. Mass Spectrom. 3 (1970) 1175.
[20] S.W. Stiller, M.V. Johnston, J. Phys. Chem. 89 (1985) 2717.
[21] T. Ast, M.A. Mabud, R.G. Cooks, Int. J. Mass Spectrom. Ion Proc. 82 (1988) 131.
[22] M.J. Hayward, M.A. Mabud, R.G. Cooks, J. Am. Chem. Soc. 110 (1988) 1343.
[23] B.E. Winger, J.R.K. Julian, R.G. Cooks, C.E.D. Chidsey, J. Am. Chem. Soc. 113 (1991) 8967.
[24] V.H. Wysocki, J.L. Jones, J.-M. Ding, J. Am. Chem. Soc. 113 (1991) 8969.
[25] T.E. Kane, Á. Somogyi, V.H. Wysocki, Org. Mass Spectrom. 28 (1993) 1665.
[26] Á. Somogyi, T.E. Kane, V.H. Wysocki, Org. Mass Spectrom. 28 (1993) 283.
[27] Á. Somogyi, T.E. Kane, J.-M. Ding, V.H. Wysocki, J. Am. Chem. Soc. 115 (1993) 5275.
[28] S.A. Miller, J.D.E. Riederer, R.G. Cooks, W.R. Cho, H.W. Lee, H. Kang, J. Phys. Chem. 98 (1994) 245.
[29] J.D.E. Riederer, R.G. Cooks, M.R. Linford, J. Mass Spectrom. 30 (1995) 241.
[30] T. Ast, T. Pradeep, B. Feng, R.G. Cooks, J. Mass Spectrom. 31 (1996) 791.
[31] B.E. Winger, H.-J. Laue, S.R. Horning, J.R.K. Julian, S.A. Lammert, D.E. Riederer, R.G. Cooks, Rev. Sci. Instrum. 63 (1992) 5613.
[32] A. Paiva, Thesis, Universidade Nova de Lisboa, 1997.
[33] Experiments have also been performed on PFPE in the tandem quadrupole, yielding similar relative intensities for the same collision energies.
[34] W.R. Koppers, J.B. Beijersbergen, T.L. Weeding, P.G. Kistemaker, A.W. Kleyn, J. Chem. Phys. 107 (1997) 10736.
[35] M. Meot-Ner (Mautner), A.R. Dongé, Á. Somogyi, V.H. Wysocki, Rapid Commun. Mass Spectrom. 9 (1995) 829.